

NANO EXPRESS

Open Access



The Effect of Decomposed PbI_2 on Microscopic Mechanisms of Scattering in $\text{CH}_3\text{NH}_3\text{PbI}_3$ Films

Dan Shan^{1,2,3}, Guoqing Tong^{1,4}, Yunqing Cao^{1,5}, Mingjun Tang², Jun Xu^{1*}, Linwei Yu¹ and Kunji Chen¹

Abstract

Hybrid organic-inorganic perovskites (HOIPs) exhibit long electronic carrier diffusion length, high optical absorption coefficient, and impressive photovoltaic device performance. At the core of any optoelectronic device lie the charge transport properties, especially the microscopic mechanism of scattering, which must efficiently affect the device function. In this work, $\text{CH}_3\text{NH}_3\text{PbI}_3$ (MAPbI₃) films were fabricated by a vapor solution reaction method. Temperature-dependent Hall measurements were introduced to investigate the scattering mechanism in MAPbI₃ films. Two kinds of temperature-mobility behaviors were identified in different thermal treatment MAPbI₃ films, indicating different scattering mechanisms during the charge transport process in films. We found that the scattering mechanisms in MAPbI₃ films were mainly influenced by the decomposed PbI_2 components, which could be easily generated at the perovskite grain boundaries (GBs) by releasing the organic species after annealing at a proper temperature. The passivation effects of PbI_2 in MAPbI₃ films were investigated and further discussed with emphasis on the scattering mechanism in the charge transport process.

Keywords: MAPbI₃ film, Hall measurement, Scattering mechanism, Grain boundary

Background

Hybrid organic-inorganic perovskite (HOIP) materials have recently emerged as highly efficient optoelectronic materials and are being intensively investigated and developed for photovoltaics, photo-detections, light-emitting diodes, and laser devices [1–6]. The perovskite solar cells have gradually emerged in the center of photovoltaic field because of their power conversion efficiency achieving over 20% during the past 8 years, as well as their cost-effective and scalable processability [7–14]. The investigations on HOIP materials (e.g., $\text{CH}_3\text{NH}_3\text{PbX}_3$, X = Cl, Br, I) have revealed their great potentials for photovoltaic applications due to optimum band gap, high absorption coefficient, high carrier mobility, and diffusion length on the order of hundreds of nanometers to micrometers in films [15–19]. At the core of any optoelectronic devices lie the electronic properties, especially the scattering mechanism governing

charge transport process. There have been many works allowing us to understand HOIP charge transport characteristics. It is apparent that the carrier mobilities of HOIP materials, which are only within the scope of 1~10 cm²/V s [20–22], are usually limited by the scattering mechanism. The $T^{-1.3}$ to $T^{-1.6}$ dependence of the mobilities on temperature have been observed by several groups, which are close to the $T^{-1.5}$ dependence usually assumed for the scattering of acoustic phonon [23, 24]. Furthermore, the scattering from grain boundaries (GBs) on charge transport in HOIPs remains unclear. The impacts of GBs with different studies usually reach conflicting conclusions. Edri et al. found a barrier in potential across the GBs in the dark, which could be reduced during the illumination [25]. Yun et al. also revealed the generation of a very small photo-voltage at GBs, but the reduced photoluminescence efficiency was found due to a deep trapping at GBs [26]. From the above introduction, we can know that although HOIP device efficiencies have increased rapidly, an understanding of the charge transport mechanisms of these materials and their underlying physical mechanisms is only starting to carry out.

* Correspondence: junxu@nju.edu.cn

¹National Laboratory of Solid State Microstructures and School of Electronic Science and Engineering and Collaborative Innovation Center of Advanced Microstructures, Nanjing University, Nanjing 210093, China
Full list of author information is available at the end of the article

In this work, the vapor solution reaction method was employed to construct compact and uniform $\text{CH}_3\text{NH}_3\text{PbI}_3$ (MAPbI₃) films. The microscopic mechanism of scattering during the charge transport process in MAPbI₃ films was evaluated via temperature-dependent Hall measurements. Two different behaviors of temperature-dependent Hall mobilities could be identified in the MAPbI₃ films before and after thermal annealing. It is confirmed that the decomposed PbI₂ located at the GBs, which is usually converted from MAPbI₃ upon thermal annealing at a proper temperature, plays an important role in the charge transport process in MAPbI₃ films. The different scattering mechanisms combining the microstructure of MAPbI₃ films were discussed, and the possible physical mechanisms were further proposed.

Methods

MAPbI₃ films were fabricated by the vapor solution reaction method as our previous works [27, 28]. The PbI₂ powder (purchased from Xi'an Polymer Light Technology Corp, 99.99%) was first dissolved in the *N,N*-dimethylformamide (DMF, Aladdin, 99.9%) solvent with a concentration of 1 mol/mL and stirred at 70 °C for 3 h. Then, the PbI₂ film was coated on the substrates by spin-coating with a speed of 4000 rpm, 30 s, and annealed at 70 °C for 10 min. The PbI₂ films and MAI powder were separately placed in two different zones of the tubular furnace equipment with a vacuum system. After pumping for 10 min, the MAI power and PbI₂ films are heated to 180 °C and 140 °C, respectively, and kept these temperatures for more than 100 min. Finally, the pre-prepared MAPbI₃ films with darkened color were annealed at different temperatures (100 °C, 120 °C, and 145 °C) for 1 h, after being washed with isopropanol. All the procedures were carried out in the open air with a humidity of ~ 45%.

The microstructures of MAPbI₃ films were measured by using X-ray diffraction (XRD) (model: MXP-III, Bruker Inc.) and scanning electron microscopy (SEM) (model: S-3400 N-II, Hitachi Inc.). The fluorescence decay curves from time-resolved photoluminescence (TRPL) measurements were recorded by a fluorescence spectrophotometer based on the time-correlated single photon counting (model: FLS920, Edinburgh Inc.). Temperature-dependent Hall measurements (model: LakeShore 8400 series, LakeShore Inc.) were performed with coplanar configurations by using Al electrodes prepared by thermal evaporation technique. Hall mobilities could be obtained from Hall effect measurements, carried out in a standard van der Pauw configuration by using an electromagnet with a magnetic induction of 0.6 T. All the temperature dependence measurements were taken during heating in the temperature range from 300 to 350 K with a step of 10 K in argon ambient.

Results and Discussion

The morphology evolution of MAPbI₃ films was firstly investigated by XRD measurement. The XRD patterns for the MAPbI₃ films before and after annealing are shown in Fig. 1. It can be clearly seen that the samples before annealing and after annealing at 120 °C are composed of pure perovskite phase, which reveals the MAPbI₃ characteristic peaks at 14.04°, 28.42°, and 43.08° corresponding to the (110), (220), and (330) planes of MAPbI₃, respectively [29]. However, it is found that the sample after annealing at 145 °C is not pure MAPbI₃ film. A new characteristic diffraction peak at 12.56° appears in the corresponding film, which could be observed by the (001) planes of PbI₂. There have been a lot of previous reports suggesting that a structural conversion from MAPbI₃ to PbI₂ occurs mostly in MAPbI₃ films upon thermal annealing [30–32]. According to these reports, we believe that MAPbI₃ films could be decomposed via heating above 145 °C in this work, where CH₃NH₃I species escape from MAPbI₃ film to form the PbI₂ phase. This indicates the weakly bonded nature between the organic and inorganic species in MAPbI₃ films [33].

The SEM images further gave a deep insight into the morphology evolution of MAPbI₃ films. In Fig. 2a–c, all the films present a compact and conformal structure. However, an amount of newly formed species occurring at GBs is emerged in the MAPbI₃ film annealed at 145 °C, which shows relatively bright contrast compared to the adjacent grains. These newly formed species have been reported previously in similar works where they were speculated to be PbI₂ components, which is consistent with the conservation of PbI₂ signals in the corresponding XRD pattern as we discussed before [33].

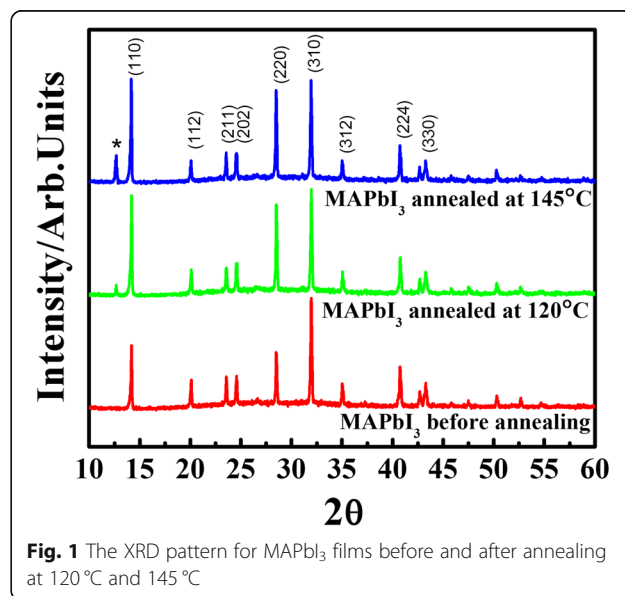


Fig. 1 The XRD pattern for MAPbI₃ films before and after annealing at 120 °C and 145 °C

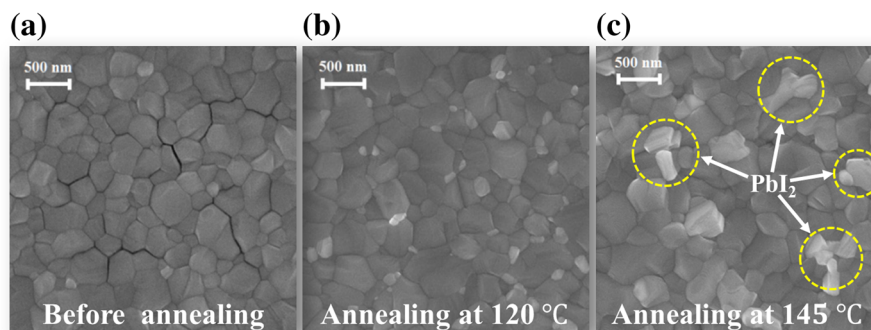


Fig. 2 The SEM images for MAPbI₃ films before (a) and after annealing at 120 °C (b) and 145 °C (c)

From these findings, we can conclude that a compositional change could occur in the MAPbI₃ film annealed above 145 °C. By releasing the organic species during annealing, PbI₂ components are decomposed and parts of them are located at the perovskite GBs according to both XRD and SEM results.

An understanding of the charge transport properties in MAPbI₃ films is highly important as the mobility usually dominates device performance. In this work, Hall mobilities of all the MAPbI₃ films were measured as shown in Fig. 3. At room temperature, Hall mobilities are around 0.6~1 cm²/V s for the unannealed, 100 °C- and 120 °C-annealed MAPbI₃ films, which are consistent with the previous reports [20, 34]. However, increased Hall mobility reaching to 5 cm²/V s is found in the 145 °C-annealed MAPbI₃ film, which is nearly one order of magnitude higher than that of the unannealed one. As we know, mobility is usually influenced by the dominant scattering mechanism governing the charge transport process. Such increased Hall mobility probably reflects a reduction of scattering during the charge transport process in the 145 °C-annealed MAPbI₃ film. Yang et al. once investigated the surfaces and GBs in MAPbI₃ films

via scanning Kelvin probe microscopy (SKPM), which is used to determine the surface potential difference between GBs and inner grains in films. It was found that the MAPbI₃ film without thermal annealing exhibited a higher surface potential at the GBs than that at the bulk, which was usually reported in the previous works [35–37]. In contrast, the surface potential at the GBs was obviously reduced after annealing at 150 °C. They considered that the decreasing of surface potential resulted from the passivation effect of newly formed PbI₂ phases, which could suppress the barrier of GBs to some extent thus reduced the scattering from GBs [33, 38]. Therefore, with the decomposed PbI₂ occurring after annealing at 145 °C in this work, the increased Hall mobility can be attributed to the passivation effect of the decomposed PbI₂ at GBs. As the Hall measurements characterize the charge transport property of the entire film, it is inferred that the decomposed PbI₂ passivates the GBs and reduces the energy barrier between grain domains, facilitating the charge transportation in the plane direction [39].

In order to further study the passivation effect of decomposed PbI₂ locating at GBs in MAPbI₃ films, temperature-dependent Hall mobilities were introduced to investigate the scattering mechanism in the MAPbI₃ films before and after annealing. Hall mobilities-temperature behaviors within the temperature range from 300 to 350 K are shown in Fig. 4a. It is clearly seen that the mobility is increased with temperature for the un- and 120 °C-annealed MAPbI₃ films. As we know, the GBs in the films with grain sizes on the micrometer scale play an important role in the charge transport process and the carrier mobility is limited by the potential energy barriers at GBs [40]. Such GBs with a large number of defects can trap the carriers and form the electrically charged states, which impede the motion of carriers from one crystallite to another and thus reduce the mobility [41]. With increasing the temperature, the carriers gain the kinetic energy to overcome the potential barriers and the carrier mobility can be increased

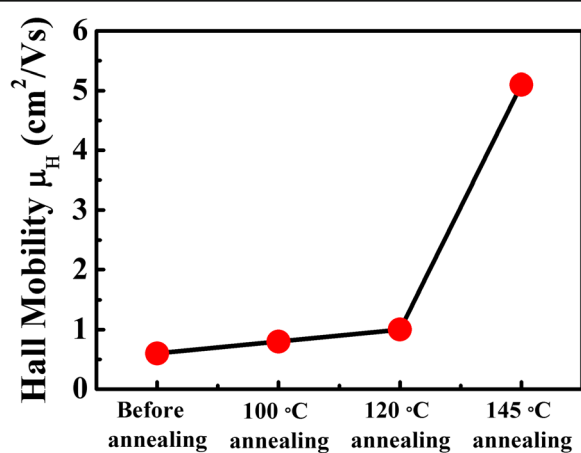


Fig. 3 Hall mobilities of all the MAPbI₃ films at room temperature

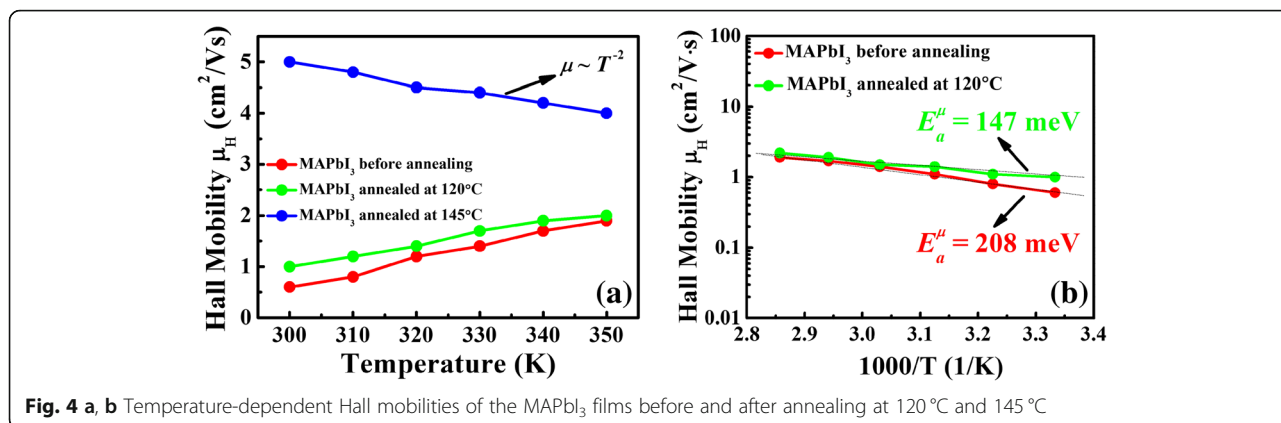


Fig. 4 a, b Temperature-dependent Hall mobilities of the MAPbI₃ films before and after annealing at 120 °C and 145 °C

accordingly [42]. Consequently, it is indicated that a GB scattering governs the charge transport process [43]. Seto et al. established the theoretical model to describe the GB scattering process and Hall mobility μ_0 shows the thermally activated behavior as below:

$$\mu_H(T) = \mu_0 \exp(-E_B/k_B T)$$

where k_B is the Boltzmann’s constant, μ_0 is the exponential prefactor, and E_B is the activation energy which corresponds to the potential energy barrier height [44]. The relationship between $\ln \mu_H$ and $1000/T$ is given within the temperature from 300 to 350 K as shown in Fig. 4b while the potential barrier height E_B of GBs can be deduced from the slope of the linear fitting. It can be found that the potential barrier height E_B of GBs is about 208 meV for the unannealed MAPbI₃ film and slightly reduces to 147 meV after annealing at 120 °C, which is almost in accordance with the previous reports [45]. However, after annealing at 145 °C, the MAPbI₃ film where the decomposed PbI₂ locating at the GBs exhibits a different temperature-dependent behavior. It is interesting to find that the mobility is decreased with the temperature increasing, which finally exhibits a $T^{-2.0}$ dependence. Such close to $T^{-1.5}$ dependence is usually assumed for the acoustic phonon scattering [23, 24]. It thus appears that the charge transport process in the 145 °C-annealed MAPbI₃ film is no longer dominated by the GB scattering, of which the acoustic phonon scattering would be instead in the charge transport process. Therefore, we could convince that the decomposed PbI₂ locating at the GBs acts as a passivation layer between the grains and suppresses the potential barrier of GBs, thus leading to the change of scattering mechanism in the charge transport process from GB scattering to acoustic phonon scattering.

Furthermore, the TRPL decay was employed and performed on the MAPbI₃ films before and after thermal

annealing, and the emission lifetime could be obtained by fitting the fluorescence emission decay spectra using the exponential function. The corresponding fluorescence emission lifetime would reflect the charge recombination behavior in the corresponding MAPbI₃ films. Figure 5 shows the TRPL decay spectra, and Table 1 displays the corresponding lifetime of MAPbI₃ films. The fluorescence emission decay curves are fitted with two-component exponential decay which exhibits the same scale of lifetime to the reported PL decay in MAPbI₃ films [46]. The fast decay component, τ_1 , might come from the surface or interface charge recombination lifetime, and the long decay component, τ_2 , could be attributed to the bulk charge recombination lifetime [47, 48]. It is found that the long decay component τ_2 shows little variation in the MAPbI₃ films before and after thermal annealing. However, the fast decay component τ_1 is increased from 1.39 ns for unannealed sample to 6.05 ns for 145 °C-annealed one, proving a reduction of surface or interface recombination,

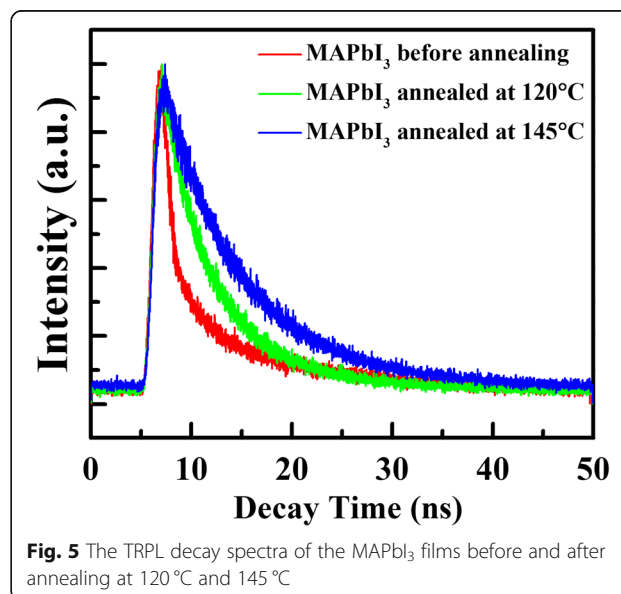


Fig. 5 The TRPL decay spectra of the MAPbI₃ films before and after annealing at 120 °C and 145 °C

Table 1 The emission lifetime of MAPbI₃ films before and after annealing at 120 °C and 145 °C

TRPL	τ_1 (ns)	τ_2 (ns)	τ (ns)
MAPbI ₃ before annealing	1.39	11.38	7.48
MAPbI ₃ annealed at 120 °C	3.02	10.48	7.72
MAPbI ₃ annealed at 145 °C	6.05	10.42	8.53

which finally results in an increase of reduced emission lifetime τ after increasing thermal annealing temperature. In the previous works, Wang et al. also investigated the charge recombination in MAPbI₃ films by analyzing the emission lifetime. They found that longer emission lifetime would indicate the enhanced suppression of the charge recombination, which could be attributed to the decomposed PbI₂ effectively passivating the charge traps at GBs in MAPbI₃ films [40]. Therefore, in this work, the enhanced τ could be ascribed to the increasing passivation effect of the decomposed PbI₂ locating at GBs which fills the GBs and suppresses the interface charge recombination in MAPbI₃ films. This is another powerful evidence for the passivation effect of the decomposed PbI₂ at the MAPbI₃ GBs.

Conclusions

In summary, MAPbI₃ films were fabricated by a vapor solution reaction method. The microstructures as well as the optical and electronic properties were investigated before and after thermally annealing. All the films show a pure perovskite phase and present typical optical properties of MAPbI₃. However, after thermal annealing at 145 °C, the decomposed PbI₂ species occurring at GBs can be revealed in MAPbI₃ films, leading to a successful passivation at GBs. Therefore, the scattering from GBs, which dominates the charge transport process in the unannealed and 120 °C-annealed MAPbI₃ films, is obviously suppressed after thermal annealing at 145 °C due to the effective passivation of PbI₂ that successfully reduces the potential barrier height of GBs. Meanwhile, the scattering from acoustic phonons turns into the prime scattering mechanism in the 145 °C-annealed MAPbI₃ film. Consequently, Hall mobility is reached to 5 cm²/V s, which is significantly higher than that of unannealed one (0.6 cm²/V s).

Abbreviations

GBs: Grain boundaries; HOIPs: Hybrid organic-inorganic perovskites; MAPbI₃: CH₃NH₃PbI₃; SEM: Scanning electron microscopy; SKPM: Scanning Kelvin probe microscopy; TRPL: Time-resolved photoluminescence; XRD: X-ray diffraction

Acknowledgements

Not applicable

Authors' Contributions

DS and JX conceived the idea and carried out the experiments. DS, GQT, YQC, and MJT participated in the preparation of the samples. DS, GQT, LWY, and JX

took part in the experiments and the discussion of the results. DS drafted the manuscript with the instruction of JX and KJC. All authors read and approved the final manuscript.

Funding

This work was supported by NSFC [grant number 61704148]; NSF of Jiangsu Province [grant number BK20170514]; "333 project" of Jiangsu Province [grant number BRA2015284]; "Qing Lan project" of Jiangsu Province; Postdoctoral research grant program of Jiangsu Province; NSF of Jiangsu Higher Education Institutions [grant number 17KJB140030]; NSF of Yangzhou City [grant number YZ2017102] and Special Fund for City School Cooperation of Yangzhou City [grant number SSX2018000001].

Availability of Data and Materials

The datasets used during the current study are available from the corresponding author of this article.

Competing Interests

The authors declare that they have no competing interests.

Author details

¹National Laboratory of Solid State Microstructures and School of Electronic Science and Engineering and Collaborative Innovation Center of Advanced Microstructures, Nanjing University, Nanjing 210093, China. ²School of Electronic and Information Engineering, Yangzhou Polytechnic Institute, Jiangsu 225127, China. ³Huafu Energy Storage New Technique Co., Ltd., Jiangsu 225600, China. ⁴Energy Materials and Surface Sciences Unit, Okinawa Institute of Science and Technology Graduate University, Okinawa, Japan. ⁵College of Physical Science and Technology, Yangzhou University, Jiangsu 225009, China.

Received: 12 January 2019 Accepted: 20 May 2019

Published online: 18 June 2019

References

- Liu J, Sheng X, Wu Y, Li D, Bao J, Ji Y, Lin Z, Xu X, Yu L, Xu J, Chen KJ (2018) All-inorganic perovskite quantum dots/p-Si heterojunction light-emitting diodes under DC and AC driving modes. *Adv Optical Mater* 6:1700897
- Green MA, Ho-Baillie A, Snaith HJ (2014) The emergence of perovskite solar cells. *Nat Photonics* 8:506–514
- Stranks SD, Snaith HJ (2015) Metal-halide perovskites for photovoltaic and light-emitting devices. *Nat Nanotechnol* 10:391–402
- Tong G, Li H, Li D, Zhu Z, Xu E, Li G, Yu L, Xu J, Jiang Y (2018) Dual-phase CsPbBr₃-CsPb₂Br₅ perovskite thin films via vapor deposition for high-performance rigid and flexible photodetectors. *Small* 14:1702523
- Tong G, Li H, Li G, Zhang T, Li C, Yu L, Xu J, Jiang Y, Shi Y, Chen KJ (2018) Mixed cation perovskite solar cells by stack-sequence chemical vapor deposition with self-passivation and gradient absorption layer. *Nano Energy* 48:536–542
- Miyasaka T (2015) Perovskite photovoltaics: rare functions of organo lead halide in solar cells and optoelectronic devices. *Chem Lett* 44:720–729
- Kojima A, Teshima K, Shirai Y, Miyasaka T (2009) Organometal halide perovskites as visible-light sensitizers for photovoltaic cells. *J Am Chem Soc* 131:6050–6051
- Lee MM, Teuscher J, Miyasaka T, Murakami TN, Snaith HJ (2012) Efficient hybrid solar cells based on meso-superstructured organometal halide perovskites. *Science* 338:643–647
- Liu M, Johnston MB, Snaith HJ (2013) Efficient planar heterojunction perovskite solar cells by vapour deposition. *Nature* 501:395–398
- Burschka J, Pellet N, Moon SJ, Humphry-Baker R, Gao P, Nazeeruddin MK, Grätzel M (2013) Sequential deposition as a route to high-performance perovskite-sensitized solar cells. *Nature* 499:316–319
- Jeon NJ, Noh JH, Kim YC, Yang WS, Ryu S, Seok SI (2014) Solvent engineering for high-performance inorganic-organic hybrid perovskite solar cells. *Nat Mater* 13:897–903
- Yang WS, Noh JH, Jeon NJ, Kim YC, Ryu S, Seo J, Seok SI (2015) High-performance photovoltaic perovskite layers fabricated through intramolecular exchange. *Science* 348:1234–1237
- Saliba M, Matsui T, Seo JY, Domanski K, Correa-Baena JP, Nazeeruddin MK, Grätzel M (2016) Cesium-containing triple cation perovskite solar cells:

- improved stability, reproducibility and high efficiency. *Energy Environ Sci* 9: 1989–1997
14. Tan H, Jain A, Voznyy O, Lan X, Arquer FPG, Fan JZ, Fan F (2017) Efficient and stable solution-processed planar perovskite solar cells via contact passivation. *Science* 355:722–726
 15. Im JH, Lee CR, Lee JW, Park SW, Park NG (2011) 6.5% efficient perovskite quantum-dot-sensitized solar cell. *Nanoscale* 3:4088–4093
 16. Baikie T, Fang Y, Kadro JM, Schreyer M, Wei F, Mhaisalkar SG, Rietzel M, White TJ (2013) Synthesis and crystal chemistry of the hybrid perovskite $\text{CH}_3\text{NH}_3\text{PbI}_3$ for solid-state sensitised solar cell applications. *J Mater Chem A* 1:5628–5641
 17. Ponceca CS, Savenije TJ, Abdellah M, Zheng K, Yartsev A, Pascher T, Harlang T, Chabera P, Pullerits T, Stepanov A, Wolf JP, Sundström V (2014) Organometal halide perovskite solar cell materials rationalized: ultrafast charge generation, high and microsecond-long balanced mobilities, and slow recombination. *J Am Chem Soc* 136:5189–5192
 18. Stoumpos CC, Malliakas CD, Kanatzidis MG (2013) Semiconducting tin and lead iodide perovskites with photonic cations: phase transitions, high mobilities, and near-infrared photoluminescent properties. *Inorg Chem* 52: 9019–9038
 19. Xing G, Mathews N, Sun S, Lim SS, Lam YM, Grätzel M, Mhaisalkar S, Sum TC (2013) Long-range balanced electron- and hole-transport lengths in organic-inorganic $\text{CH}_3\text{NH}_3\text{PbI}_3$. *Science* 342:344–347
 20. Wehrenfennig C, Eperon GE, Johnston MB, Snaith HJ, Herz LM (2014) High charge carrier mobilities and lifetimes in organolead trihalide perovskites. *Adv Mater* 26:1584–1589
 21. Dong QF, Fang YJ, Shao YC, Mulligan P, Qiu J, Cao L, Huang JS (2015) Electron-hole diffusion lengths > 175 μm in solution grown $\text{CH}_3\text{NH}_3\text{PbI}_3$ single crystals. *Science* 347:967–970
 22. Shi D, Adinolfi V, Comin R, Yuan MJ, Alarousu E, Buin A, Chen Y, Hoogland S, Rothenberger A, Katsiev K, Losovsky Y, Zhang X, Dowben PA, Mohammed OF, Sargent EH, Bakr OM (2015) Low trap-state density and long carrier diffusion in organolead trihalide perovskite single crystals. *Science* 347:519–522
 23. Savenije TJ, Ponceca JCS, Kunneman L, Abdellah M, Zheng K, Tian Y, Yartsev A (2014) Thermally activated exciton dissociation and recombination control the carrier dynamics in organometal halide perovskite. *J Phys Chem Lett* 5:2189–2194
 24. Karakus M, Jensen SA, Angelo FD, Turchinovich D, Bonn M, Cánovas E (2015) Phonon-electron scattering limits free charge mobility in methylammonium lead iodide perovskites. *J Phys Chem Lett* 6:4991–4996
 25. Edri E, Kirmayer S, Henning A, Mukhopadhyay S, Gartsman K, Rosenwaks Y, Hodes G, Cahen D (2014) Why lead methylammonium tri-iodide perovskite-based solar cells require a mesoporous electron transporting scaffold (but not necessarily a hole conductor). *Nano Lett* 14:1000–1004
 26. Yun JS, Baillie AH, Huang SJ, Woo SH, Heo Y, Seidel J, Huang FZ, Cheng YB, Green MA (2015) Benefit of grain boundaries in organic-inorganic halide planar perovskite solar cells. *J Phys Chem Lett* 6:875–880
 27. Tong GQ, Lan XZ, Song ZH, Li GP, Li H, Yu LW, Xu J, Jiang Y, Sheng Y, Shi Y, Chen KJ (2017) Surface-activation modified perovskite crystallization for improving photovoltaic performance. *Materials Today Energy* 5:173–180
 28. Tong GQ, Geng XS, Yu YQ, Yu LW, Xu J, Jiang Y, Sheng Y, Shi Y, Chen KJ (2017) Rapid, stable and self-powered perovskite detectors via a fast chemical vapor deposition process. *RSC Adv* 7:18224
 29. Cao DH, Stoumpos CC, Malliakas CD, Katz MJ, Farha OK, Hupp JT, Kanatzidis MG (2014) Remnant PbI_2 , an unforeseen necessity in high-efficiency hybrid perovskite-based solar cells? *Appl Materials* 2:091101
 30. Supasai T, Rujisamphan N, Ullrich K, Chemseddine A, Ditttrich T (2013) Formation of a passivating $\text{CH}_3\text{NH}_3\text{PbI}_3/\text{PbI}_2$ interface during moderate heating of $\text{CH}_3\text{NH}_3\text{PbI}_3$ layers. *Appl Phys Lett* 103:183906
 31. Jacobsson TJ, Correa-Baena JP, Anaraki EH, Philippe B, Stranks SD, Bouduban M, Tress W, Schenk K, Teuscher J, Moser JE, Rensmo H, Hagfeldt A (2016) Un-reacted PbI_2 as a double-edged sword for enhancing the performance of perovskite solar cells. *J Am Chem Soc* 138:10331–10343
 32. Wang S, Dong W, Fang X, Zhang Q, Zhou S, Deng Z, Tao R, Shao J, Xia R, Song C, Hu L, Zhu J (2016) Credible evidence for the passivation effect of remnant PbI_2 in $\text{CH}_3\text{NH}_3\text{PbI}_3$ films in improving the performance of perovskite solar cells. *Nanoscale* 8:6600–6608
 33. Chen Q, Zhou HP, Song TB, Luo S, Hong ZR, Duan HS, Dou LT, Liu YS, Yang Y (2014) Controllable self-induced passivation of hybrid lead iodide perovskites toward high performance solar cells. *Nano Lett* 14:4158–4163
 34. Walsh A, Scanlon DO, Chen SY, Gong XG, Wei SH (2015) Self-regulation mechanism for charged point defects in hybrid halide perovskites. *Angew Chem Int Ed Engl* 54:1791–1794
 35. Dymshits A, Henning A, Segev G, Rosenwaks Y, Etgar L (2015) The electronic structure of metal oxide/organometal halide perovskite junctions in perovskite based solar cells. *Sci Rep* 5:8704
 36. Ono LK, Qi YB (2016) Surface and interface aspects of organometal halide perovskite materials and solar cells. *J Phys Chem C* 7:4764–4794
 37. Li H, Tong GQ, Chen TT, Zhu HW, Li GP, Chang YJ, Wang L, Jiang Y (2018) *J Mater Chem A* 6:14255–14261
 38. Chatterjee S, Pal AJ (2016) Introducing Cu_2O thin films as a hole-transport layer in efficient planar perovskite solar cell structures. *J Phys Chem C* 120:1428–1437
 39. Shao YC, Xiao ZG, Bi C, Yuan YB, Huang JS (2014) Origin and elimination of photocurrent hysteresis by fullerene passivation in $\text{CH}_3\text{NH}_3\text{PbI}_3$ planar heterojunction solar cells. *Nat Commun* 5:5784
 40. Saidaminov MI, Abdelhady AL, Murali B, Alarousu E, Burlakov VM, Peng W, Dursun I, Wang L, He Y, Maculan G (2015) High-quality bulk hybrid perovskite single crystals within minutes by inverse temperature crystallization. *Nat Commun* 6:7586
 41. Nussbaumer H, Baumgartner FP, Willeke G, Bucher E (1998) Hall mobility minimum of temperature dependence in polycrystalline silicon. *J Appl Phys* 83:292–296
 42. Seto JYW (1975) The electrical properties of polycrystalline silicon films. *J Appl Phys* 46:5247–5254
 43. Shan D, Qian MQ, Ji Y, Jiang XF, Xu J, Chen KJ (2016) The change of electronic transport behaviors by P and B doping in nano-crystalline silicon films with very high conductivities. *Nanomaterials* 6:233
 44. Scheller LP, Nickel NH (2012) Charge transport in polycrystalline silicon thin-films on glass substrates. *J Appl Phys* 112:013713
 45. Thomas MB, David AE, Leeor K, Gary H, David C (2016) Hybrid organic-inorganic perovskites: low cost semiconductors with intriguing charge transport properties. *Nat Rev Mater* 1:15007
 46. Wang L, McCleese C, Kovalsky A, Zhao Y, Burda C (2014) Femtosecond time-resolved transient absorption spectroscopy of $\text{CH}_3\text{NH}_3\text{PbI}_3$ perovskite films: evidence for passivation effect of PbI_2 . *J Am Chem Soc* 136:12205–12208
 47. Gunawan O, Todorov TK, Mitzi DB (2010) Loss mechanisms in hydrazine-processed $\text{Cu}_2\text{ZnSn}(\text{Se}, \text{S})_4$ solar cells. *Appl Phys Lett* 97:233506
 48. Huang J, Shao Y, Dong Q (2015) Organometal trihalide perovskite single crystals: a next wave of materials for 25% efficiency photovoltaics and applications beyond? *J Phys Chem Lett* 6:3218–3227

Publisher's Note

Springer Nature remains neutral with regard to jurisdictional claims in published maps and institutional affiliations.

Submit your manuscript to a SpringerOpen[®] journal and benefit from:

- Convenient online submission
- Rigorous peer review
- Open access: articles freely available online
- High visibility within the field
- Retaining the copyright to your article

Submit your next manuscript at ► springeropen.com